The Cockayne syndrome group A and B proteins are part of a ubiquitin–proteasome degradation complex regulating cell division

Elena Paccosi[a,1], Federico Costanzo[b,1], Michele Costantino[a], Alessio Balzerano[a], Laura Monteonofrio[c], Silvia Soddu[c], Giorgio Prantera[d], Stefano Brancorsini[e], Jean-Marc Egly[b,f,2], and Luca Proietti-De-Santis[a,2]

[a]Unit of Molecular Genetics of Aging, Department of Ecology and Biology, University of Tuscia, 01100 Viterbo, Italy; [b]Department of Functional Genomics and Cancer, Institut de Génétique et de Biologie Moléculaire et Cellulaire, Equipe Labellisée Ligue contre le Cancer (IGBMC), CNRS/INSERM/University of Strasbourg, BP163, Illkirch Cedex, 67404 Strasbourg, France; [c]Unit of Cellular Networks and Molecular Therapeutic Targets, Istituto di ricovero e cura a carattere scientifico (IRCCS) Regina Elena National Cancer Institute, 00144 Rome, Italy; [d]Epigenetics and Developmental Genetics Laboratory, Department of Ecology and Biology, University of Tuscia, 01100 Viterbo, Italy; [e]Unit of Molecular Pathology, Department of Experimental Medicine, section of Terni, University of Perugia, 06100 Perugia, Italy; and [f]Department of Toxicology, College of Medicine, National Taiwan University, 10051 Taipei City, Taiwan

Edited by Philip C. Hanawalt, Stanford University, Stanford, CA, and approved October 14, 2020 (received for review April 14, 2020)

Cytokinesis is monitored by a molecular machinery that promotes the degradation of the intercellular bridge, a transient protein structure connecting the two daughter cells. Here, we found that CSA and CSB, primarily defined as DNA repair factors, are located at the midbody, a transient structure in the middle of the intercellular bridge, where they recruit CUL4 and MDM2 ubiquitin ligases and the proteasome. As a part of this molecular machinery, CSA and CSB contribute to the ubiquitination and the degradation of proteins such as PRC1, the Protein Regulator of Cytokinesis, to ensure the correct separation of the two daughter cells. Defects in CSA or CSB result in perturbation of the abscission leading to the formation of long intercellular bridges and multinucleated cells, which might explain part of the Cockayne syndrome phenotypes. Our results enlighten the role played by CSA and CSB as part of a ubiquitin/proteasome degradation process involved in transcription, DNA repair, and cell division.

Cockayne syndrome | cytokinesis | cell division | abscission | ubiquitination

CSA and CSB were at first characterized as playing a role in transcription-coupled repair (TCR), the subpathway of nucleotide excision repair (NER), specifically aimed at the removal of DNA bulky adducts located on the transcribed strand of active genes (1). During TCR, CSA and CSB proteins first participate in the removal of the RNA polymerase stalled in front of the lesion (2, 3) and then in the recruitment of NER proteins, including the transcription/DNA repair factor TFIIH (4, 5). *CSA* and *CSB* mutations result in Cockayne syndrome (CS) (6, 7), a human autosomal recessive disorder characterized by a variety of clinical features, including growth deficiency and severe neurological and developmental manifestations (8). However, it has become increasingly clear that some of the features exhibited by CS patients could hardly be attributed to DNA repair deficiencies and that CSA and CSB functions extend far beyond their role in DNA repair. In fact, the inability of the ultraviolet (UV)-irradiated CS cells to rapidly recover their normal RNA synthesis was shown to be not solely due to the persistence of damage per se, since even nondamaged genes were switched off (9). In transcription, CSB was shown to stimulate RNA polymerases activity (10–13). CSB harbors an ATPase activity and is a member of the SWI2/SNF2 family of chromatin remodelers (14, 15). CSA belongs to the family of WD-40 repeat proteins, known for coordinating interactions among multiprotein complexes (16), and is a component of a ubiquitin E3 ligase complex containing CUL4, RBX1, and DDB1 (17, 18). In line with this, it was also found that CSA, as part of the ubiquitin/proteasome machinery together with CSB, was responsible for the resumption from transcription arrest in UV-treated cells (19). In the latter case, CSA and CSB were involved in the ubiquitination and further degradation of ATF3, a DNA binding protein that transcriptionally represses a large number of genes upon cellular stress. Moreover, recent work underlines a connection between UV stress response and the fate of RNA polymerase, the latter accordingly subjected to an ubiquitination process signaling its further degradation (20–22).

During cell division, the cytoplasm of a single eukaryotic cell divides into two daughter cells, a phenomenon called cytokinesis (23). Cytokinesis begins in the early stages of anaphase, after chromosome segregation, and requires the assembly of an actin–myosin contractile ring, which shrinks the plasma membrane between the newly formed nuclei and compacts the midzone microtubules to form the midbody. The midbody is a transient structure located in the center of the intercellular bridge connecting the two daughter cells at the end of cytokinesis (24). It is then the resolution of the intercellular bridge, through the severing of the microtubules localized at the midbody, a process known as abscission, to define the end of the process (25, 26). Abscission requires a series of dynamic events, including midbody-targeted vesicle trafficking, specialization of plasma membrane domains, disassembly of

Significance

Here, we demonstrate that CSA and CSB proteins, primarily defined as DNA repair factors, are part of a ubiquitin/proteasome degradation process during cytokinesis. Both CSA and CSB localize at the midbody, a transient structure located at the intercellular bridge, where they recruit a ubiquitination/proteasomal degradation complex for the degradation of PRC1, thus allowing the separation of the daughter cells. Defects in CSA or CSB result in perturbation of the abscission, leading to cytokinesis defects that might explain part of the Cockayne syndrome phenotypes. Our results enlighten the role played by CSA and CSB in a ubiquitin/proteasome degradation process involved not only in transcription and DNA repair, but also in cell division.

Author contributions: E.P., F.C., M.C., L.M., S.S., G.P., J.-M.E., and L.P.-D.-S. designed research; E.P., F.C., M.C., A.B., and L.P.-D.-S. performed research; L.M., S.S., S.B., and J.-M.E. contributed new reagents/analytic tools; and E.P., F.C., G.P., J.-M.E., and L.P.-D.-S. wrote the paper.

The authors declare no competing interest.

This article is a PNAS Direct Submission.

[1]E.P. and F.C. contributed equally to this work.

[2]To whom correspondence may be addressed. Email: egly@igbmc.fr or proietti@unitus.it.

This article contains supporting information online at https://www.pnas.org/lookup/suppl/doi:10.1073/pnas.2006543117/-/DCSupplemental.

First published November 16, 2020.

midbody-associated microtubule bundles, and plasma membrane fission (27, 28).

Here, in order to unveil new functions of CS proteins that could explain part of the very severe and complex phenotype exhibited by CS patients (29, 30), we analyzed the dynamic localization of CS proteins during cell division. Surprisingly, we observed that CSA and CSB localize at the midbody to recruit additional factors and initiate the ubiquitination and degradation of proteins such as PRC1, thus leading to the successful separation of the two daughter cells. We also demonstrate that loss of function of CS proteins, as well as knockdown of their ubiquitin ligase partners CUL4 and MDM2, disturbs cytokinesis, highlighting their crucial role in cell division.

Results

CSA and CSB Proteins Localize at the Midbody. Confocal microscopy using well-characterized antibodies (9, 19, 29) showed that, in HeLa cells, endogenously expressed CSB and CSA localized within the intercellular bridge and specifically at midbody (95.3 ± 1.5% and 95 ± 2.6%, respectively; $n = 100 \times 3$ experiments (exp.), here highlighted by staining with α-tubulin (Fig. 1 *A* and *B*, *a–c*). In contrast, the fluorescence signal was rarely detected either for CSB (2.3 ± 0.5%; $n = 100 \times 3$ exp.) in siRNA *CSB*-silenced HeLa cells or for CSA (2.3 ± 1.5%; $n = 100 \times 3$ exp.) in siRNA *CSA*-silenced HeLa cells (Fig. 1 *A* and *B*, *d–f*). Similarly, in CS patients-derived CS1AN and CS3BE cells (that don't express endogenous CSB and CSA proteins, respectively; *Materials and Methods* and *SI Appendix*, Fig. S1), CSB and CSA signal was always absent at the midbody (Fig. 1 *C* and *D*, *a–c*). On the contrary, in CS1AN/CSBwt and CS3BE/CSAwt rescued cells, obtained by stably expressing the respective wild-type proteins (31) (*SI Appendix*, Fig. S1), both CSB (82.3 ± 4%; $n = 100 \times 3$ exp.) and CSA (84 ± 7%; $n = 100 \times 3$ exp.) proteins localized within the intercellular bridge at midbody, here highlighted by staining with the Aurora B kinase (32) (Fig. 1 *C* and *D*, *d–f*).

To exclude nonspecific off-target effects of the antibodies raised against CS proteins, we transiently expressed wild-type GFP-CSB and GFP-CSA tagged proteins in CS1AN and CS3BE cells, respectively. GFP fluorescence showed that both fusion proteins GFP-CSB (77.2 ± 2.1%; $n = 100 \times 2$ exp.) and GFP-CSA (81 ± 4.2%; $n = 100 \times 2$ exp.) were found at the midbody, here stained with anti-PLK1, a serine/threonine kinase localized at the central region of the spindle in late mitosis (*SI Appendix*, Fig. S2 *A* and *C*), while GFP protein alone was never detectable at the midbody (*SI Appendix*, Fig. S2 *B* and *D*). Localization of endogenous CSA and CSB protein at the midbody was also confirmed in other cell lines such as SKNBE-2c and MCF7 (*SI Appendix*, Fig. S2 *E–H*).

The discovery that CSB and CSA proteins, so far considered strictly as nuclear proteins, were located at the midbody, led us to investigate their dynamic localization during the cell cycle progression. As schematized in *SI Appendix*, Fig. S3*A*, CSB and CSA, both located in the nucleus during interphase (*SI Appendix*, Fig. S3 *B* and *C*, *a*), migrated to the external boundary of the spindle midzone (stained by Aurora B) in late anaphase, during cleavage furrow contraction (*SI Appendix*, Fig. S3 *B* and *C*, *b*). At telophase, CSB was found in a characteristic ring-like arrangement surrounding the midbody in the so called "bulge zone," while CSA localized in the "dark zone," a narrow region sited in the center of the midbody (*SI Appendix*, Fig. S3 *B* and *C*, *c–e*).

As CSA and CSB were found to be part of a protein ubiquitination/degradation mechanism (19, 33), we hence investigated the localization of their partners at the midbody. Confocal microscopy showed that both CUL4 and MDM2 ubiquitin ligases, known to be CSA interactors (17, 34), localized at the midbody in both CSB-rescued (84.3 ± 2.5% and 85.6 ± 3%, respectively; $n = 100 \times 3$ exp.) and CSA-rescued (81.3 ± 2.5% and 91 ± 4%, respectively; $n = 100 \times 3$ exp.) cells (Fig. 1 *E–H*, *a–c*), whether their recruitment was impaired in CSA-deficient (15.5 ± 6% and 14 ± 7.5%, respectively; $n = 100 \times 3$ exp.) cells (Fig. 1 *F* and *H*, *d–f*). On the contrary, in CSB-deficient cells (in which CSA is expressed), both CUL4 and MDM2 recruitment at the midbody (83 ± 5.6% and 79 ± 8.8%, respectively; $n = 100 \times 3$ exp.) remained unaffected (Fig. 1 *E* and *G*, *d–f*).

Interestingly, we next observed that CSA is recruited at the midbody in both CSB-deficient and CSB-rescued cells (92.1 ± 1.6% and 94 ± 1.5%, respectively; $n = 100 \times 3$ exp.) (Fig. 1 *I*, *d–f* and *a–c*, respectively). Furthermore, silencing of CSB in HeLa cells does not affect CSA recruitment at the midbody (Fig. 1 *J*, *a–c*; 90.3 ± 3.6%) as compared to the ones transfected with the scramble siRNA (Fig. 1 *J*, *d–f*; 95 ± 1.4%).

CSA and CSB Interacting Partners at the Midbody. To further localize CSA and CSB, we prepared protein fractions from purified midbodies, (the last shown by confocal microscopy, *SI Appendix*, Fig. S4*A*) from CSB- and CSA- deficient (CS1AN and CS3BE) and CSB- and CSA-rescued (CS1AN/CSBwt and CS3BE/CSAwt) telophase-enriched proliferating cells. In this fraction, we then found both CSB and CSA proteins, together with other midbody structural components, as well as α-tubulin, which was enriched in its acetylated form (Fig. 2 *A* and *B*, lanes 3 and 6). The quality of our midbody preparation was further proven by the lack of actin and transcription factor Sp1 (here used as markers of cytoplasmic and nuclear contamination, respectively) in the midbody fraction, that were instead detected in total protein extracts from asynchronous and telophase-enriched cells. As an additional negative control, we found that XPA, another DNA repair protein, was not present in the midbody fraction.

Moreover, PRC1 antibody immune-precipitated CSB and CSA proteins as well as CUL4, a CSA partner, from CS1AN, CS1AN/CSBwt, CS3BE and CS3BE/CSAwt midbody extracts (Fig. 2 *C* and *D*, lane 5). Interestingly, both CSA and CUL4 coprecipitate with PRC1 in the absence of CSB (Fig. 2*C*, lane 4). In corroboration with immunofluorescence studies (Fig. 1 *F*, *d–f*), immunoprecipitation (IP) studies showed a slight decrease of CUL4 in the PRC1 immunoprecipitated fractions in the absence of CSA (Fig. 2*D*, lane 4). As a control, nonspecific (IgG) antibodies were unable to immune-precipitate either CSB or CSA in the respective CS1AN and CS3BE cell extracts (Fig. 2 *C* and *D*, lane 3). Reciprocal immunoprecipitation studies confirmed that PRC1 coeluted in a protein fraction together with CSA, CSB, and CUL4 proteins (*SI Appendix*, Fig. S4 *B* and *C*)

The above data underlined the presence at the midbody of a protein ubiquitin machinery containing CSA, CSB, and CUL4 associated with PRC1. Confocal microscopy next pointed out that PRC1, normally localized in the dark zone in CS1AN/CSBwt- and CS3BE/CSAwt-rescued cells (Fig. 3 *A* and *B*, *a–c*), was found progressively delocalized to both arms of the intercellular bridge in CS1AN and CS3BE cells, either at the same point of the cell cycle in which normal rescued cells exhibited the secondary ingression (Fig. 3 *A* and *B*, *d–f*) or at the late point of cytokinesis when the intercellular bridge became abnormally long (Fig. 3 *A* and *B*, *g–i*) (37.5 ± 3.5% in CS1AN and 39.5 ± 6.3 in CSS3B; $n = 100 \times 3$ exp.). This abnormal pattern appeared to be strongly specific for PRC1, as other proteins such as polo-like kinase 1 (PLK1), mitotic kinesin-like protein 1 (MLPK1), centrosomal protein 55 (CEP55), and ALG-2-interacting protein X (Alix), all of them being involved in cytokinesis, were found correctly localized (in the dark zone of the midbody), in both the normal and long intercellular bridges (*SI Appendix*, Fig. S5).

In addition, knockdown of either CUL4 or MDM2 (*SI Appendix*, Fig. S6*A*), in both CS1AN/CSBwt and CS3BE/CSAwt also resulted in the delocalization of PRC1 all along the elongated intercellular bridge, thus mimicking the phenotype observed in CS-deficient cells (Fig. 3 *C–F*).

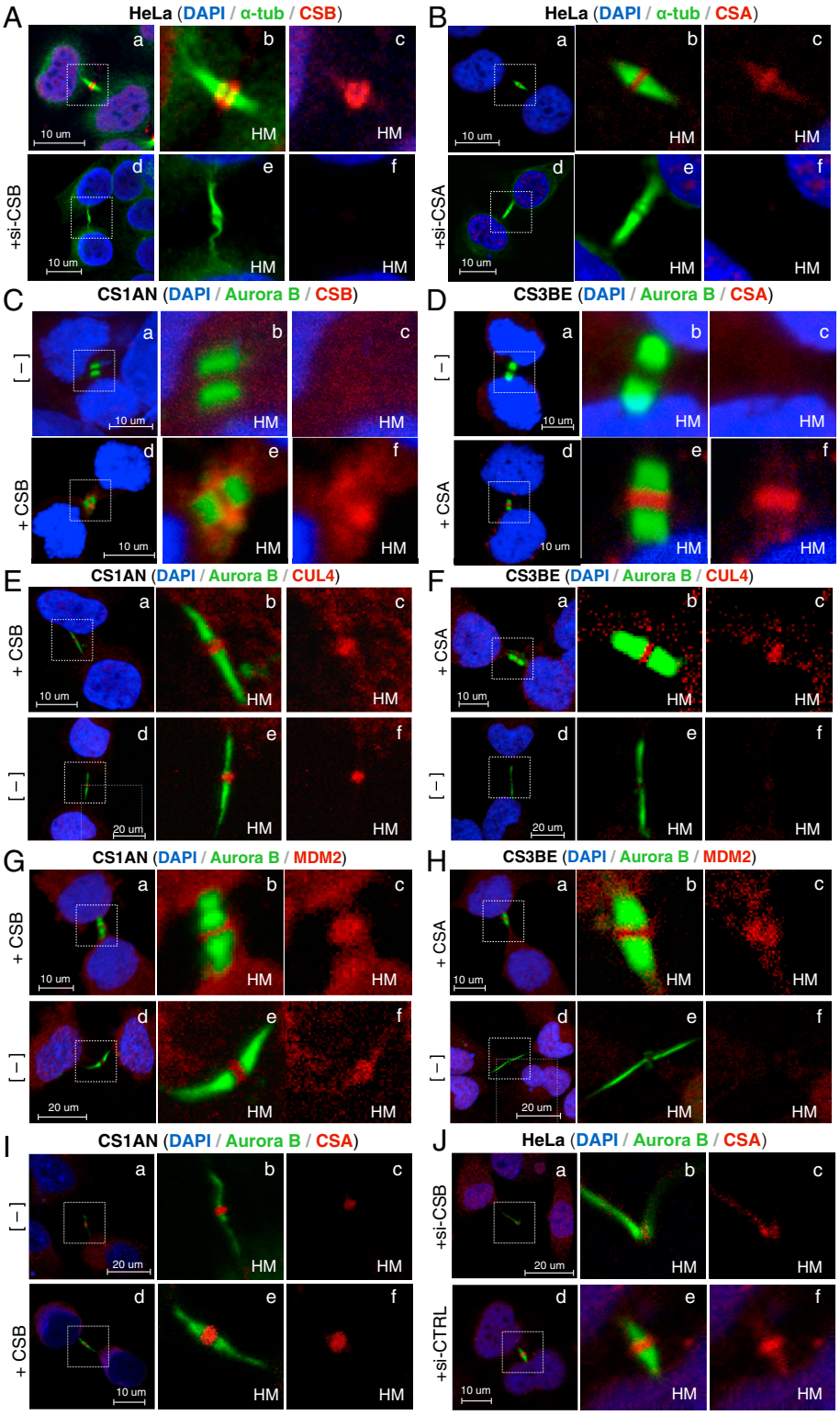

Fig. 1. CSA, CSB, and their partners localize at the midbody. Confocal micrographs of HeLa (*A* and *B*), HeLa/siCSB (*A*, *d–f*), and HeLa/siCSA (*B*, *d–f*) cells stained for DNA (blue), α-tubulin (α-tub) (green), and endogenous CSB (*A*), or CSA (*B*) (red). Confocal micrographs of CS1AN [–] and CS1AN/CSBwt rescued (+CSB) (*C*, *E*, and *G*) as well as of CS3BE [–] and CS3BE/CSAwt rescued (+CSA) (*D*, *F*, and *H*) stained for DNA (blue), Aurora B (green), and either CSB (*C*), CSA (*D*), CUL4 (*E* and *F*), or MDM2 (*G* and *H*) (red). Confocal micrographs of CS1AN [–] and CS1AN/CSBwt rescued (+CSB) (*I*), stained for DNA (blue), Aurora B (green), and endogenous CSA (red). Confocal micrographs of HeLa/siCSB (*J*, *a–c*) and HeLa/siCTRL (*J*, *d–f*) cells stained for DNA (blue), Aurora B (green), and endogenous CSA (red). HM indicates high magnification of relative dotted square area.

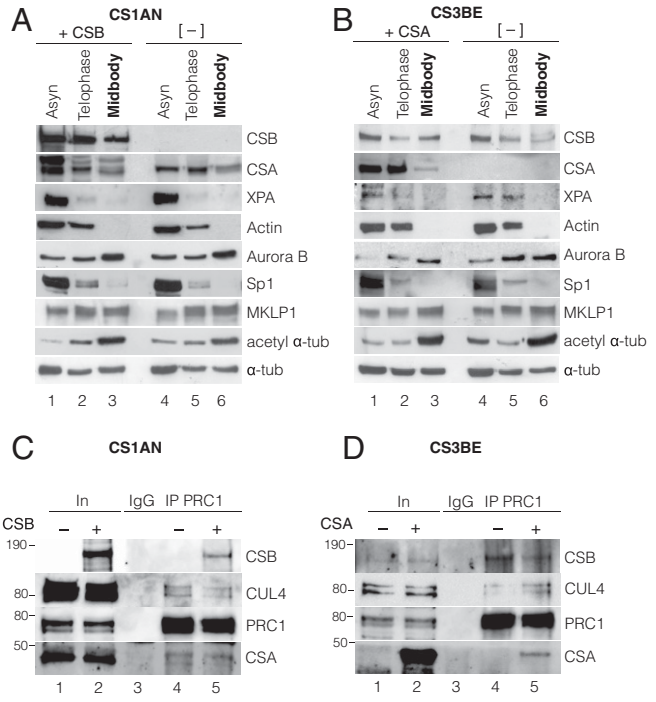

Fig. 2. CSA and CSB interact with CUL4 and PRC1. Cell fractionation assay showing asynchronous total cellular extract (Asyn), telophase-enriched total cellular extract, and midbody fraction from CS1AN/CSBwt rescued (+CSB) and CS1AN [–] (*A*) as well as CS3BE/CSAwt rescued (+CSA) and CS3BE [–] (*B*). Western blots have been performed with antibodies against CSB, CSA, XPA, Actin, Aurora B, MKLP1, Sp1, acetylated α-tubulin (acetyl α-tub), and α-tubulin (α-tub). Immunoprecipitation of PRC1 (IP PRC1) from CS1AN [–] and CS1AN/CSBwt-rescued midbody fraction (*C*) as well as CS3BE [–] and CS3BE/CSAwt-rescued midbody fraction (*D*). Immunoprecipitation with nonspecific antibody (IgG) has been used as negative control. Input (In) stands for 10% of the lysate used for the IP. Western blots have been performed using antibodies against CSB, CSA, PRC1, and Cul4. Each Western blot is the representation of three independent biological repeats.

CSA and CSB Are Engaged in an Ubiquitination Process. We next investigated whether, in CS-deficient cells, the formation of aberrant long intercellular bridges, in which PRC1 appears to be delocalized, was due to its improper ubiquitination. We then performed proximity ligation assay (PLA), that allows detection of closely related interacting polypeptides (in this case ubiquitin and PRC1) to analyze in situ ubiquitination of PRC1. We observed PLA-positive spots of PRC1 ubiquitination in CS3BE/CSAwt (CSA rescued) cells (54 ± 4.2%; $n = 30 \times 2$ exp.) cells (Fig. 3 *G*, *a* and *b*; Fig. 3*H*, histograms), while the presence of these spots was dramatically reduced in CS3BE cells (2.5 ± 0.7%; $n = 30 \times 2$ exp.) cells (Fig. 3 *G*, *c* and *d*; Fig. 3*H*, histograms). Interestingly, PRC1 ubiquitination also occurred in CS1AN (63.5 ± 2.7%; $n = 30 \times 2$ exp.) (Fig. 3 *G*, *e* and *f*; Fig. 3*H*, histograms), regardless of CSB functionality, thus demonstrating that ubiquitination of PRC1 is CSA dependent.

To biochemically visualize PRC1 ubiquitination, both CSA- and CSB-deficient (CS3BE and CS1AN) and CSA- and CSB-rescued (CS3BE/CSAwt and CSIAN/CSBwt) cells were transfected with PRC1-pEGFP-C2 vector (expressing GFP-tagged PRC1) and pEBB-BT-ubiquitin vector (expressing ubiquitin tagged with a biotinylation site) and further supplemented with biotin. After assessing that ectopic expression of ubiquitin was similar across all of the samples (*SI Appendix*, Fig. S6*C*), we performed PRC1 pull-down from midbody extracts with GFP-trap beads, followed by blotting against either biotin or PRC1 (Fig. 3 *I* and *J*). This experiment revealed that the ubiquitination of PRC1 strongly depends on the presence of CSA (Fig. 3*I*, lanes 1 and 2) but not of CSB, even if CSB expression seems to further increase the rate of ubiquitination (compare lanes 4 and 5) in particular with regard to the higher molecular weight (MW) (polyubiquitinated forms). Moreover, we observed that silencing of CUL4 (*SI Appendix*, Fig. S6*B*) dramatically impaired the ubiquitination of PRC1 in both CSA and CSB rescued cells (Fig. 3 *I* and *J*, lanes 3 and 6).

To further investigate the role of CSA in ubiquitinating PRC1, we set up an in vitro ubiquitination assay using PRC1 as a substrate, recombinant MDM2, and immune-purified CSA. In those conditions, PRC1 was ubiquitinated in the presence of either MDM2 or CSA (*SI Appendix*, Fig. S6*C*, lanes 2 and 3); when both MDM2 and CSA were added together, we noticed a slight increase in the ubiquitination signal at higher MW.

Altogether, the above data strongly suggest the involvement of both CSA and CSB together with CUL4 and MDM2 E3 ubiquitin ligases in a ubiquitination process at the midbody that used PRC1 as a substrate.

PRC1 Is Degraded in a CSA- and CSB-Dependent Manner. We were next wondering whether the ubiquitination of PRC1 at the midbody would have preceded its degradation. Immunofluorescence studies showed that the non-ATPase regulatory subunit 1 (PSMD1) of the 26S proteasome complex was present at the midbody in both CSA-deficient and -rescued (88 ± 5.2% and 87.3 ± 8.1%, respectively; $n = 100 \times 3$ exp.) cells (CS3BE/CSAwt) (Fig. 4*B*). In CSB-rescued cells (CS1AN/CSBwt), PSMD1 was found at the midbody (65.3 ± 7.1%; $n = 100 \times 3$ exp.) while in CSB-deficient (8.3 ± 2.5% ; $n = 100 \times 3$ exp.) cells, it was hardly detectable (Fig. 4*A*, compare *a–c* and *d–f*), suggesting a pivotal and likely specific role of CSB in recruiting the proteasome.

Immunoprecipitation assays from CSB proficient midbody extracts revealed that PRC1 coeluted with PSMD1 (Fig. 4*C*). Moreover, the ubiquitin immune-precipitated fraction from the same midbody extracts was shown to contain PSMD1, suggesting the engagement of the proteasome machinery within the midbody (Fig. 4*D*). To further investigate the fate of PRC1 up to the completion of cytokinesis, CS3BE, CS1AN, CS3BE/CSAwt, and CS1AN/CSBwt cells were synchronized and midbody extracts were collected at different times after the release from the prometaphase block. In WT (CS1AN/CSBwt and CS3BE/CSAwt) cells, we observed a progressive PRC1 degradation (Fig. 4 *E* and *F*, lanes 5 through 8) which was completed after 3 h (180 min) and correlated with a faithful abscission within the same time (*SI Appendix*, Fig. S7 *A* and *C* and Movie S1), whereas in CS cells, PRC1 failed to be degraded (Fig. 4 *E* and *F*, lanes 1 through 4), and consequently the presence of long intercellular bridges and a delay/failure of abscission is observed (*SI Appendix*, Fig. S7 *A* and *D* and Movie S2).

Analysis of cyclin B1 amount (*SI Appendix*, Fig. S8 *A* and *B*) along the entire time course confirmed the effective synchronization of cells and demonstrated that the persistence of PRC1, in CS-deficient cells, was not due to a delay in cell cycle progression (relative quantification is showed in the graphs, Fig. 4 *G* and *H*).

We also set up an in vitro degradation assay, in which recombinant PRC1 was incubated over time with telophase-enriched total extracts from either CS1AN, CS3BE cells as well as CS1AN/CSBwt- and CS3BE/CSAwt-rescued cells. In rescued cell extracts, PRC1 underwent a progressive degradation along the incubation time, which was almost completed after 180 min (Fig. 4 *I* and *J*, lanes 1 through 5, and the corresponding graphs). On the contrary, in CS-deficient cells, PRC1 degradation was significantly impaired (lanes 6 through 10).

Altogether, the above data demonstrated that CSA and CSB are part of a ubiquitin/proteasome degradation process that targets the PRC1 protein present at the midbody. Interestingly,

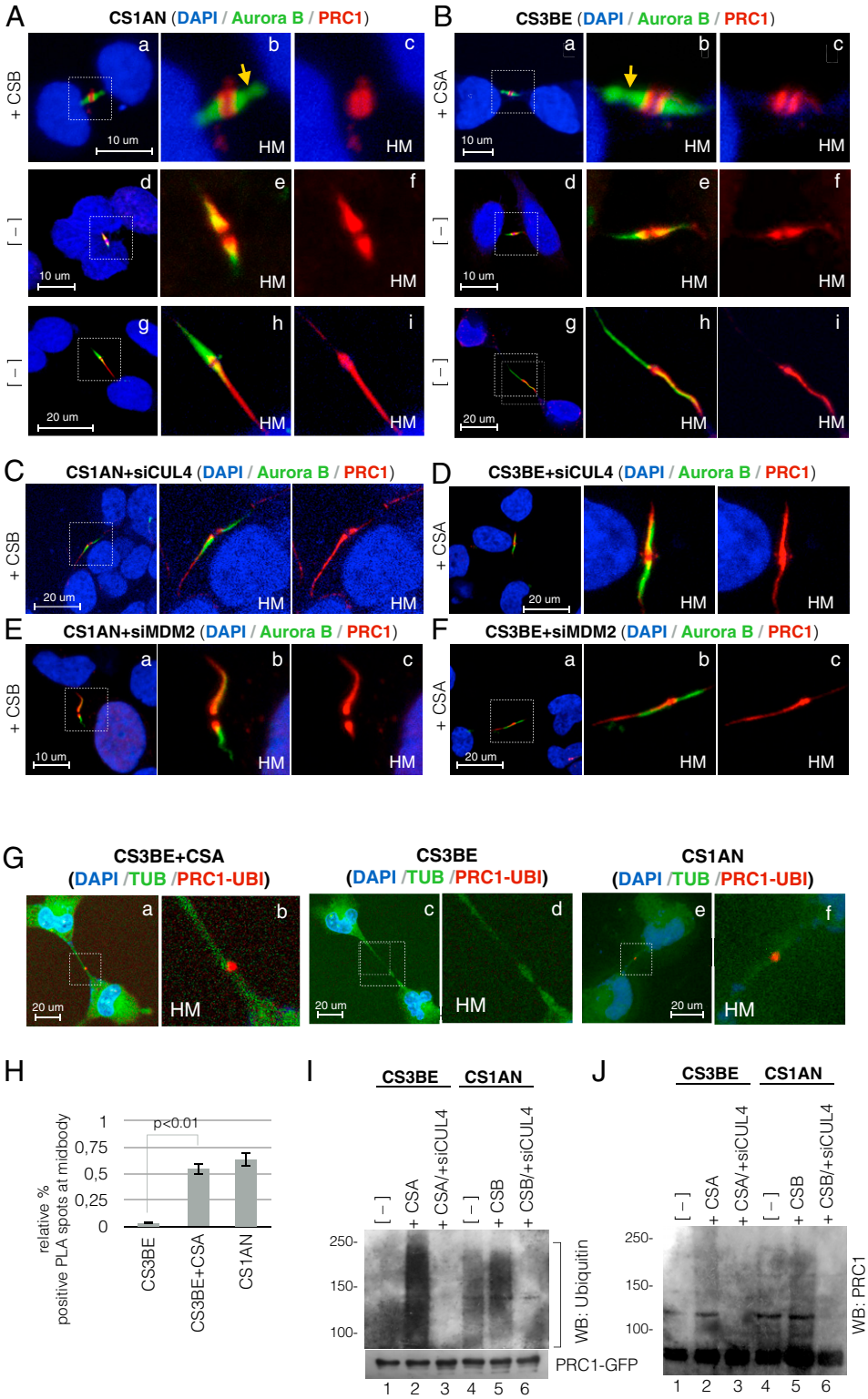

Fig. 3. CSA and CSB proteins are involved in the ubiquitination of PRC1. Confocal micrographs of CS1AN [–] and CS1AN/CSBwt rescued (+CSB) (*A*), CS3BE [–] CS3BE/CSAwt rescued (+CSA) (*B*), CS1AN/CSBwt rescued/siCUL4 (+CSB) (*C*), CS3BE/CSAwt rescued/siCUL4 (+CSA) (*D*), as well as CS1AN/CSBwt rescued/siMDM2 (+CSB) (*E*) and CS3BE/CSAwt rescued/siMDM2 (+CSA) (*F*), stained for DNA (blue), Aurora B (green), and PRC1 (red). Confocal micrographs of CS3BE [–], CS3BE/CSAwt rescued (+CSA), and CS1AN [–] stained for DNA (blue) and tubulin (green) (*G*) showing PLA of PRC1 ubiquitination. Ubiquitination of PRC1 is revealed by red spots. HM indicates high magnification of relative dotted square area. Graphs showing relative percentage of PLA positive spots at midbody (*H*). Data are presented as means (±SD) of three independent experiments. Immunoprecipitation of PRC1-GFP from pEBB-BT transfected (ubiquitin) CS3BE [–], and CS3BE/CSAwt-rescued (+CSA) as well as CS1AN [–] and CS1AN/CSBwt-rescued (+CSB) and CS3BE/CSAwt rescued/siCUL4 (+CSA) and CS1AN/CSBwt-rescued/siCUL4 (+CSB) midbody extracts. Western blot has been performed using antibodies against PRC1 and biotin (*I*) or only PRC1 (*J*). Each Western blot is the representation of three independent biological repeats.

although they work in concert, it seems that CSA is devoted to the ubiquitination process, and CSB to the recruitment of the proteasome machinery.

CSB and CSA Defects Resulted in Binucleated Cells and Multipolar Mitotic Spindles. We hence wondered how a defect in CSA- and CSB-dependent ubiquitination/proteasome degradation impacts cytokinesis. In CSB- and CSA-deficient cells, we found a significant amount (at least three and eight times more, respectively; P value <0.01) of binucleated cells (Fig. 5 *A* and *B* and histograms Fig. 5 *E* and *H*). The same phenomenon was observed in CSA- and CSB-rescued cells after either suppression of CUL4 (siCUL4) or treatment with MG132 proteasome inhibitor (Fig. 5 *E* and *H*, respectively). We also observed a significant increase (P value <0.01) of multipolar mitosis in CS-deficient cells, when compared with CS-rescued cells (Fig. 5 *C* and *D* and histograms Fig. 5 *F* and *I*). Moreover, long intercellular bridges (LIBs) between daughter cells (as illustrated in Fig. 3 *A*–*F*) were found in significant amounts in CSA- and CSB-deficient cells as well as in siCUL4 or siMDM2 cells (*SI Appendix*, Fig. S9 *A* and *B*). Accordingly, in CSA- and CSB-deficient cells as well as in siCUL4 and siMDM2 WT cells, we noticed a significant increase in the average length of the bridges (Fig. 5 *G* and *J*), pointing out the formation of LIBs as a specific feature of CS cells, linked to the prolonged presence of PRC1 at the midbody. Conversely, LIBs were not observed after suppression of PRC1, which instead gave rise to mitotic abnormalities, such as furrow regression and aberrant spindle formation (*SI Appendix*, Fig. S10 *A*, *B*, *F*, and *G*, lanes 1 and 2).

Overall, the above features strongly indicated a cytokinesis failure in CSA- and CSB-deficient cells and highlighted the detrimental consequences of the loss of CSA and CSB function for proper cell division.

Discussion

Cytokinesis, the final step of cell division, requires a complex assembly of proteins that are finely tuned by posttranslational modifications, such as phosphorylation/dephosphorylation, sumoylation, ubiquitination, and polymerization/ depolymerization, which ultimately leads to a successful abscission. The present study demonstrates that, during cytokinesis, CSA and CSB are recruited at the midbody to develop their ubiquitin-dependent degradation activity aimed to trigger the abscission of the two daughter cells.

Abscission Requires CSA and CSB. Our results compellingly indicate that, in addition to their nuclear localization in interphase, which is in accordance with their functions in DNA repair and transcription, CSA and CSB migrate, during late telophase, at the midbody, to exert, together with the E3 ubiquitin ligases MDM2 and CUL4 and the proteasome, the ubiquitin-dependent degradation of PRC1, a main component of the intercellular bridge (35). During this process, CSA and CSB play concerted but distinct roles. Indeed, CSA promotes the recruitment of CUL4 and MDM2 ubiquitin ligases (Fig. 1 *F*–*H*) to further ubiquitinate their targeted substrate (PRC1), whereas CSB contributes to the recruitment of the proteasome, as observed by the presence of PMSD1 (Fig. 4 *A*–*C*). In vivo and in vitro experiments demonstrate that PRC1 ubiquitination (Fig. 3 *G*–*J* and *SI Appendix*, Fig. S6*B*) and proteasomal degradation (Fig. 4 *F*, *H*, and *J*) are CSA dependent. Similarly, in absence of CSB, PRC1 is not degraded (Fig. 4 *E*, *G*, and *I*), even if properly ubiquitinated (Fig. 3 *G*–*J* and *SI Appendix*, Fig. S6*B*). Interestingly, we showed that ubiquitination of PRC1 also depends on CUL4 ubiquitin ligase. Of note, the role of CUL4 and MDM2 ubiquitin ligases in cooperation with CS proteins showed that: 1) their presence at the midbody was dependent on CSA (Fig. 1 *F*–*H*); and 2) their siRNA-mediated depletion gave rise to cellular phenotypes similar to what was observed in absence of either CSA or CSB (Fig. 5 *G* and *J*). It cannot be excluded that MDM2 might partially substitute for CSA/CUL4 ubiquitination. Moreover, we also noticed that the PRC1 degradation pathway is CSA/CSB dependent, which is not the case for cyclin B1 degradation, that occurs even in CS-deficient cells (Fig. 4 *E*–*H* and *SI Appendix*, Fig. S8 *A* and *B*).

Although immunofluorescence and functional studies suggest distinct and sequential roles for CSA and CSB during the ubiquitination and the degradation of PRC1, we cannot exclude an intimate partnership between them along the different stages of cytokinesis. Indeed, pull-down from CSB- and CSA-rescued midbody extracts revealed coelution of CSB and CSA (*SI Appendix*, Fig. S11*C*), and PLA experiments revealed how the two CS proteins transiently interact together at the midbody (*SI Appendix*, Fig. S11*A*). Moreover, immunoprecipitation experiments show that either CSB or CSA (including CUL4) coelute with PRC1 (Fig. 2 *C* and *D*). However, we failed to observe the coelution of PRC1 with both CSA and CSB, suggesting that CS proteins might interact sequentially with PRC1.

It thus seems that this study points out the unexpected and specific role of CSA and CSB as part of a ubiquitin/proteasome degradation process involved in abscission, a key step of cytokinesis.

Mitotic Defects and Cytokinesis Failure in CS Cells. The removal of PRC1 from the midbody seems to be absolutely required to fully accomplish cytokinesis: An inefficient degradation of PRC1 at the midbody, as observed following the impairment of either CSA or CSB, prevents abscission and results, in a striking increase, in binucleated cells, in multipolar mitosis, and a significant increment and number of LIBs (Fig. 5). This situation is comparable with that observed when PRC1 or the yeast homolog ASE1 was overexpressed (35, 36). It is likely that defects in PRC1 degradation might prevent spindle central microtubule disassembly to fully complete abscission (24).

Unfortunately, silencing PRC1 does not restore the wild-type phenotype. Indeed, PRC1 appears to be absolutely required before cytokinesis onset, during the anaphase–telophase transition, for spindle midzone formation and completion of mitosis (36, 37). Here, silencing of PRC1 (*SI Appendix*, Fig. S10 *D* and *E*) impairs cleavage furrow completion, leading to mitotic defects such as furrow regression (illustrated in *SI Appendix*, Fig. S10 *A* and *B*, *a* and *c*) and chromosomal bridges formation (illustrated in *SI Appendix*, Fig. S10 *A* and *B*, *b* and *d*), that prevent cytokinesis entering, regardless of CS protein functionality. Results and statistical significance are graphed in *SI Appendix*, Fig. S10 *F* and *G* (lanes 1 and 2). In contrast, these mitotic defects were not observed in CS-deficient cells where, instead, the resulting lack of PRC1 degradation during cytokinesis led to abscission defects, highlighted by the strong increase of cells presenting long intercellular bridges (illustrated in *SI Appendix*, Fig. S10 *C*, *a* and *b*, and graphed in *SI Appendix*, Fig. S10 *F* and *G*, lane 3).

Therefore, the need of a tight and fine tuning of PRC1 amount during the different steps of cell division seems to be crucial for cleavage furrow completion, during mitosis, but detrimental for the successful completion of cytokinesis. Here, we demonstrated that, at the late step of cytokinesis, elimination of PRC1 promotes abscission, being that its persistence would presumably impact the severing of microtubules required in the final step of abscission. It is not clear what the mechanism is that determines the spreading of PRC1 along the intercellular bridge, when not properly degraded at the midbody, as observed in CS-deficient cells (Fig. 3 *A* and *B*) or after CUL4 and MDM2 siRNA-mediated depletion (Fig. 3 *C* and *D*). Interestingly, the same phenomenon (spreading and accumulation of PRC1 along the intercellular bridge) has recently been observed after depletion

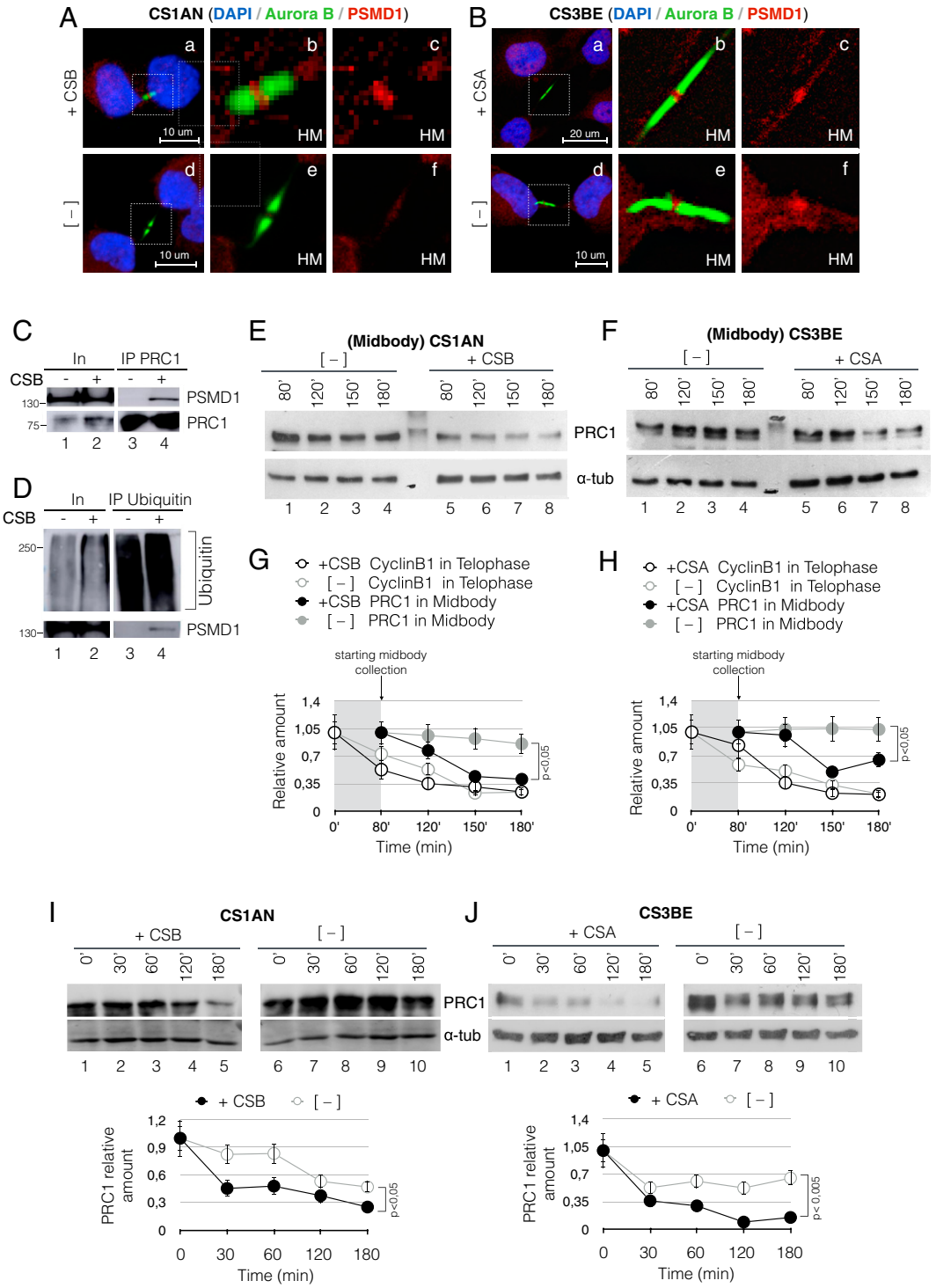

Fig. 4. The recruitment of ubiquitin/proteasome machinery at midbody is disturbed in the absence of CS proteins. Confocal micrographs of CS1AN [–] and CSIAN/CSBwt rescued (+CSB) (*A*) as well as CS3BE [–] and CS3BE/CSAwt rescued (+CSA) (*B*) stained for DNA (blue), Aurora B (green), and PSMD1 (red). HM indicates high magnification of relative dotted square area. PSMD1 does not localize to the midbody during cytokinesis in 19.8 ± 1.5% SD of CS3BE [–] cells ($n = 500$) and in 55.6 ± 2.4% SD of CS1AN [–] cells ($n = 500$). Immunoprecipitation of PRC1 (IP PRC1) (*C*) as well as ubiquitin (IP ubiquitin) (*D*) from CS1AN [–] and CS1AN/CSBwt-rescued (+CSB) telophase-enriched extracts. Western blot has been performed using antibodies against PSMD1, ubiquitin, and PRC1. Cell lysates from CS1AN [–] and CSIAN/CSBwt-rescued (+CSB) (*E*) as well as CS3BE [–] and CS3BE/CSAwt-rescued (+CSA) (*F*) midbody extracts. Western blot has been performed using antibodies against PRC1 and α-tubulin (α-tub). Graphs showing relative amount of PRC1 (filled circles) in midbody extracts and Cyclin B1 (open circles) in telophase total cellular extracts in CS1AN [–] and CSIAN/CSBwt rescued (+CSB) (*G*) as well as in CS3BE [–] and CS3BE/CSAwt rescued (+CSA) (*H*). Times after release from prometaphase block are indicated. Data are presented as means (±SD) of three independent experiments. In vitro degradation assay in the presence of recombinant PRC1 and lysates from CS1AN/CSBwt-rescued (+CSB) and CSIAN [–] (*I*) as well as CS3BE/CSAwt-rescued (+CSA) and CS3BE [–] (*J*) extracts. Western blot has been performed using antibodies against PRC1 and α-tubulin (α-tub). Times after release from prometaphase block are indicated. Respective line charts represent quantified PRC1 relative amount. Values are from three independent biological repeats (mean ± SD; one-way ANOVA with Tukey's post hoc test was used for statistical analysis).

of midbody components such as PP1β-MYPT1 and MKLP1 (38). We also might wonder whether accumulation of PRC1 often occurring in only one arm of the LIB (33.2 ± 3.4%, $n = 100 \times$ exp. in CSA-deficient cells and 40.4 ± 5.1%, $n = 100 \times 3$ exp. in CSB-deficient cells), was the result of an "asymmetric dissociation" process giving rise to two separate daughter cells with a midbody remnant (39, 40).

We cannot exclude that other mitotic defects, like cleavage furrow regression or chromosome bridge formation, instead of cytokinesis failure, likewise followed by tetraploidization (41), could give rise to the observed multipolar cells. Significantly however, in CS cells, we observed neither mitotic defects (*SI Appendix*, Fig. S10 *F* and *G*, lane 3) nor a delay in metaphase–anaphase transition (*SI Appendix*, Fig. S7*B*) but, instead, we observed both a dramatic increase of dividing cells exhibiting LIBs and a strong extension of metaphase–abscission time, indicative of a primary effect of CSA and CSB depletion on the last step of cytokinesis. However, we should point out that the fate of LIB-carrying cells is not necessarily binucleation: in certain cases, the cells become permanently blocked in cytokinesis and finally undergo cell death (*SI Appendix*, Fig. S10*H*). Alternatively, in a number of cases, the prolonged traction forces between the two daughter cells exhibiting LIBs can lead to mechanical resolution of the bridge (*SI Appendix*, Fig. S12*B* and Movie S4).

Finally, it is possible that additional compensatory effects, able to overcome the defect observed in CS cells, might somehow help faithful cytokinesis. Indeed, other factors might be recruited to eliminate components of the intercellular bridge and to assure the completion of cytokinesis. Interestingly, various E3 ligases seem to be required for some of the sequential steps that govern cytokinesis and the ubiquitination/degradation of components of the midbody, such as APC/C^{Cdh1} that targets Aurora B and Plk1 (42, 43). Accordingly, depletion of other pivotal components of the intercellular bridge such as Alix, CEP55, and ESCRT-III/VPS4 proteins, also results in cytokinetic abscission failure (44, 45).

The Pleiotropic Role of CSA and CSB: DNA Repair, Transcription, and Cell Division. While they have been initially considered as factors only involved in transcription-coupled repair (1), CSA and CSB turn out to be involved in additional processes mainly related to transcription: they control the levels of p53 after different cellular stresses (46); they participate in the recovery of RNA synthesis after the massive transcriptional shutdown induced upon genotoxic stress (9, 19, 47); and they positively control transcription of rDNA genes and ribosome biogenesis (48). Moreover, CSBs cooperate with c-JUN to regulate transcription and chromatin modification (49). It also should be pointed out the role of CSA and CSB in RNA pol I transcription and ribosomal biogenesis (11, 12, 50–53). Along this line, recently, CSA was shown to induce ubiquitination of nucleolin, a nucleolar protein that regulates rRNA synthesis and ribosome biogenesis (48). Furthermore, CS proteins were shown to play a role in mitochondrial metabolism, i.e., stimulation of mitochondrial DNA repair (54) and transcription (55) as well as regulation of proteostasis (56) and signaling (57, 58).

Here we demonstrate a role of CSA and CSB in exploiting their ubiquitin/proteasome degradation activity for the fine tuning of the last step of cytokinesis, the abscission. Our results thus provide additional clues for the understanding of the clinical and cellular phenotypes of Cockayne syndrome that could not be solely attributed to DNA repair and transcription deficiencies. Indeed, we evidenced how CS-deficient cells undergo cytokinesis failure, thus leading to the formation of binucleated cells, a feature previously associated with cellular senescence (59) and proliferative arrest (60), even in absence of DNA damage. Altogether, these abnormalities may trigger progeria-related features observed in CS, such as the premature subcutaneous fat loss (61) that account for the dramatic cachexia displayed by the patients, but also for the overall cell depletion.

Interestingly, similar phenotypes are present in other disorders characterized by abscission defects, like Fanconi anemia, in which the depletion of bone marrow cells suffered by patients is due to apoptosis of multinucleated cells (62), or Lowe syndrome, in which cataracts and osteopenia stem from cell depletion after abscission failure (63).

To summarize, the present work establishes the role of CSA and CSB as part of a ubiquitin/proteasome degradation machinery involved in several mechanisms that control cellular life, e.g., DNA repair, transcription, and cell division.

Materials and Methods

Cells and Culture Conditions. MCF-7 cells were grown in Dulbecco's modified Eagle medium (DMEM) supplemented with 10% fetal bovine serum (FBS), 2 mM L-glutamine and 0.6 μg/mL of insulin from bovine pancreas. HeLa cells were grown in DMEM supplemented with 10% FBS and 2 mM L-glutamine. SKNBE-2c cells were grown in minimum essential medium (MEM)/DMEM F12 medium supplemented with 10% FBS and 2 mM L-glutamine.

CS1AN is an immortalized CSB-null line derived from a severely affected individual CS1AN, a compound heterozygote consisting of one *CSB* allele with an early truncating mutation (K337STOP) and a second allele with a 100-nt deletion in exon 13 (7). CS3BE is an immortalized CSA line derived from a severely affected individual CS3BE, a compound heterozygote consisting of one *CSA* allele with a missense mutation (A160V) and a nonsense mutation (E13X) (64). CSIAN/CSBwt and CS3BE/CSAwt cells are stably transfected with constructs for conditional expression of the respective WT protein (19). Protein expression levels in WT and rescued cells are shown in *SI Appendix*, Fig. S1. CS1AN, CS3BE, CS1AN/CSBwt, and CS3BE/CSAwt cells were grown in DMEM/F10 medium supplemented with 10% FBS and 2 mM L-glutamine.

Cell Synchronization. Cells were synchronized with 100 ng/mL nocodazole for 3 h and released to reach the defined mitotic stages.

Western Blot. Proteins were fractionated by sodium dodecyl sulfate/polyacrylamide gel electrophoresis (SDS/PAGE) and transferred to Protran nitrocellulose membranes (Sigma) and blotted with respective antibodies.

Midbody Isolation and Extraction. Cells were synchronized with nocodazole and released until telophase. Midbodies were isolated as described by Kuriyama et al. (65). Briefly, culture medium was supplemented with 5 μg/ml Taxol (Sigma) before harvest. Cell pellets were then resuspended in spindle isolation buffer (2 mM Pipes [pH 6.9], 0.25% Triton X-100, and 20 μg/mL Taxol) and incubated at room temperature. Protein extraction from sedimented midbodies was performed with extraction buffer (50 mM Tris·HCl [pH 7.4], 600 mM NaCl, 0.1% SDS, 0.5% Nonidet P-40, 1 mM dithiothreitol (DTT), 5 mM ethylenediaminetetraacetic acid (EDTA) supplemented with protease- and phosphatase-inhibitor mix (Roche). Total cellular extracts from nonsynchronized cells were treated in the same manner.

Cytospin. Diluted samples were run, following manufacturer instructions into a cytospin centrifuge at 500 rpm for 5 min. Slides containing spun cells, were washed three times with phosphate-buffered saline (PBS) before immunofluorescence procedure.

Immunofluorescence Microscopy. For immunofluorescence experiments, cells were seeded onto Ibidi coverslips. Cells were fixed in ice-cold methanol or 2% formaldehyde, washed three times in PBS, permeabilized in 0.25% Triton X-100 in PBS for 10 min, and then blocked in 3% bovine serum albumin in PBS for 30 min before the required primary Abs were applied. The following Abs were employed: anti-Aurora B moAb (AIM-1) (BD Biosciences), anti-alpha-tubulin moAb (Sigma), rabbit anti-gamma-tubulin Ab (Sigma), rabbit anti-CSB (N2C1), Internal Ab (GeneTex), rabbit anti-ERCC8 [N2C2], Internal Ab (GeneTex), rabbit anti-PLK1 Ab (Santa Cruz Biotechnology), anti-MDM2 moAb (Santa Cruz Biotechnology), rabbit anti-PSMD1 Ab (Abcam), rabbit anti-CUL4 Ab (Santa Cruz Biotechnology), rabbit anti-PRC1 Ab (Santa Cruz Biotechnology), rabbit anti-MKLP1 Ab (Santa Cruz Biotechnology), mouse anti-Alix Ab (Santa Cruz Biotechnology), mouse anti-Cep55 Ab (Santa Cruz Biotechnology), and rabbit cleaved caspase-3 (Asp175) (Cell Signaling). Appropriate secondary Alexa Fluor Abs (Thermo Fisher Scientific) were used.

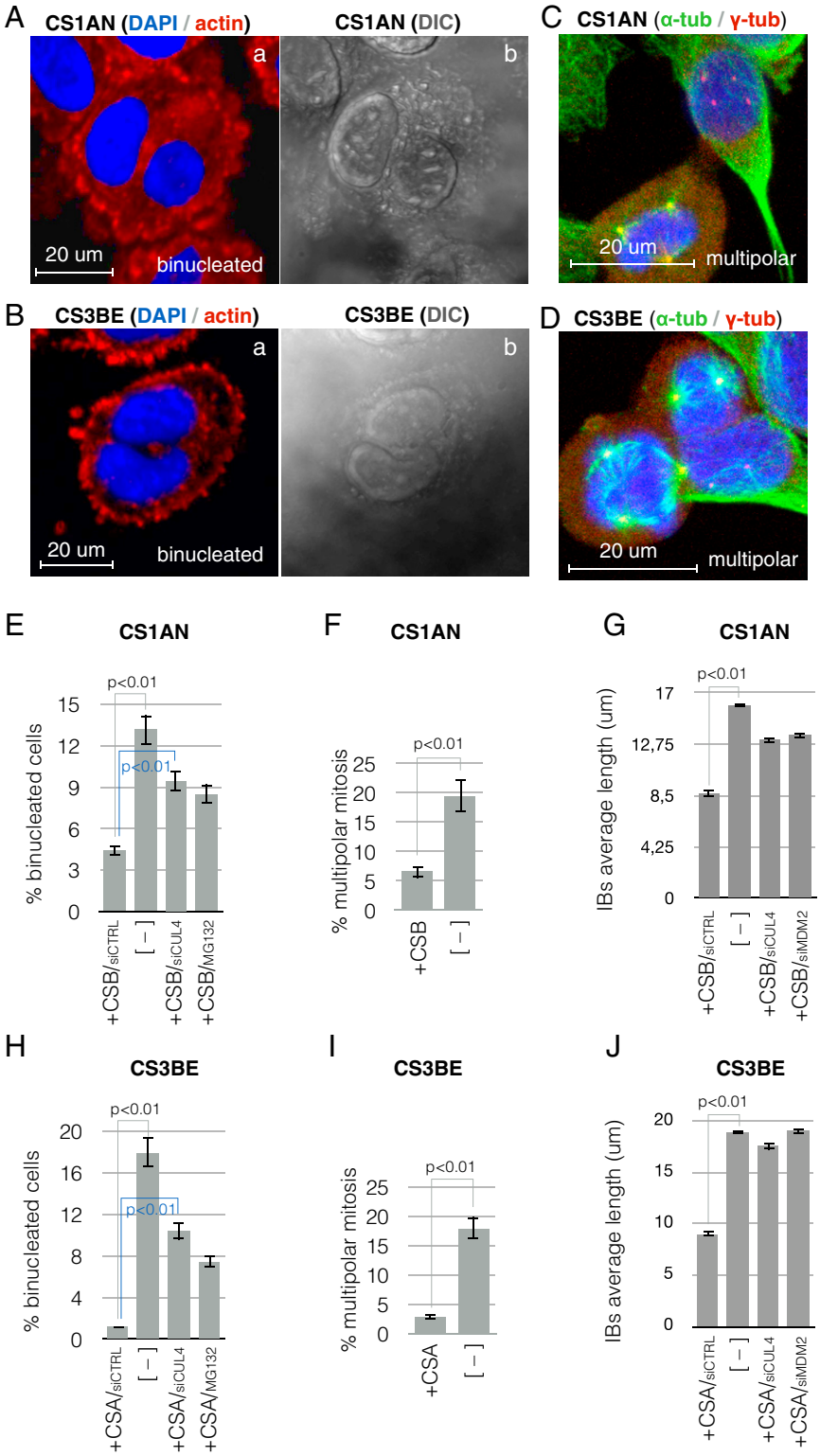

Fig. 5. CSB and CSA deficiency causes binucleation and multipolar mitosis. Confocal micrographs and differential interference contrast (DIC) images of CS1AN (*A*) and CS3BE (*B*) cells, stained for DNA (blue) and actin (red). Confocal micrographs of CS1AN (*C*) and CS3BE (*D*) cells, stained for DNA (blue), α-tubulin (green), and γ-tubulin (red). Histograms showing the frequencies of the indicated mitotic defects (*E*, *F*, *H*, and *I*). Histograms showing intercellular bridges average length (*G* and *J*). Data are presented as means (±SD) of three independent experiments.

DNA was marked with 4′,6-diamidino-2-phenylindole (DAPI) in Vectashield. Slides were analyzed with a confocal microscope system (Zeiss LSM 710) and images were acquired using the interfaced software ZEN 2010: both microscope hardware and software configuration were always maintained. Technical parameters fixed in our acquisition procedure were pinhole size, at 1 AU (Airy unit), laser power at 2%, and digital gain at 1.0. Images were then processed using ImageJ software, in order to merge channels from monochrome acquisitions and make montage, when serial microscope scans of the specimen were performed along *z* axis.

Plasmid and siRNA Transient Transfection. For transient protein expression, plasmid DNA was added to the cells for 48 h using Xtreme gene 9 reagent (Roche). For RNA interference RNA oligonucleotides (Dharmacon) targeting CSA and CSB mRNA (siRNA) were transfected in HeLa cells at a concentration of 100 nM, while a pool of four RNA oligonucleotides (Dharmacon) targeting MDM2, CUL4, and PRC1 mRNA (siRNA) was transfected in CS3BE/CSAwt or CS1AN/CSBwt cells at a concentration of 100 nM. A pool of RNA oligonucleotides without any target mRNA (siCtrl) was used as control. Cells were fixed 48 h after transfection. siRNA transfection was performed using Lipofectamine 2000 transfection reagent (Thermo Fisher), according to the manufacturer's instructions.

Immunoprecipitation Assay. CSA-3×FLAG-TY1 or CSB-TY1 protein expression was induced for 24 h by addition of doxycycline to the CS3BE/CSA3×FLAG-TY1 or CS1AN/CSB-TY1 cells (19). Cells were lysed in IP buffer (50 mM Hepes [pH 7.5], 100 mM NaCl, 0.2% Nonidet P-40, 0.5% Na-deoxycholate, 15% glycerol) supplemented with protease-inhibitor mix (Roche), and sonicated before lysate clearance. Pull-down was carried out using anti ERCC8 (Abcam), CSB 3222 (IGBMC) coupled to magnetic protein G beads overnight at 4 °C. For PRC1, immunoprecipitation was carried out by using either PRC1 antibody (Santa Cruz) or PRC1 AC resin (Santa Cruz). Immunoprecipitation with GFP-trap beads (ChromoTek) was performed by incubating them at 4 °C overnight with midbody extracts from cell transfected with both pEBB-BT ubiquitin (Addgene no. 36098) and PRC1-pEGFP-C2 (Addgene no. 6083-1) vectors and then cultured in a medium supplemented with 4 μM D-biotin (Sigma). GFP-trap beads were separated from supernatant by centrifugation and beads were thoroughly washed with IP buffer before the elution procedure.

In Vitro Ubiquitination Assay. Reactions were performed in a 60-μL mixture containing PRC1-His Tag protein (Sino Biological), 1× ubiquitin conjugation reaction buffer (B70), 1× Mg-ATP solution (B-20), 1 mM ubiquitin (U-100H), 50 nM ubiquitin-activating enzyme (UBE1-E305), 250 nM UbcH5c (E2-627), where indicated His-MDM2 (E3-200), all purchased from Boston Biochem and, where indicated, immunopurified CSA. After 2 h of incubation at 37 °C, reaction mixtures were separated by SDS/PAGE and analyzed by immunoblotting using PRC1 antibody.

In Vivo Detection of Ubiquitinated Proteins. CS3BE, CS3BE/CSAWT, CS1AN, and CS1AN/CSBWT were transfected with pEBB-BT ubiquitin vector (Addgene no. 36098). A total of 4 μM D-biotin (Sigma) was added to the medium. Lysis was performed as described (66). Briefly, cells were lysed in a (2% SDS, 150 mM NaCl, 10 mM Tris·HCl [pH 8.0]) buffer at the indicated times, boiled for 10 min, and then sonicated with standard conditions. Cleared lysates were then diluted 10 times in dilution buffer (10 mM Tris·HCl [pH 8.0], 150 mM NaCl, 2 mM EDTA, 1% Triton). Extracts were incubated overnight with Dynabeads streptavidin (Thermo) or PRC1-AC resin (Sigma). Immunoprecipitated biotinilated ubiquitinated proteins were washed 2 times in washing buffer (10 mM Tris·HCl [pH 8.0], 1 M NaCl; 1 mM EDTA, 1% Nonidet P-40) and eluted by boiling 10 min in 2× loading buffer. Samples were resolved in Criterion TGX (Tris-Glycine eXtended) precast gels (Bio-Rad). Blots were incubated with antibody against biotin (Santa Cruz, 39-15D9), ubiquitin (Santa Cruz, A-5), and PRC1 (Abcam, ab51248).

Protein Degradation Assay. Fresh telophase-enriched cell lysates were prepared from CS3BE or CS1AN (CSA or CSB expression was induced by addition of doxycycline for 8 h). Cells were lysed in degradation buffer D (25 mM Tris·HCl [pH 7.5], 10 mM MgCl2, 150 mM NaCl, 15% glycerol) and sonicated; the cell extracts were then cleared by centrifugation, and complemented by Energy Regeneration Solution. The purified PRC1-His Tag protein (Sino Biological) was added to the reaction and amounts of sample were taken at indicated time points. Reaction was carried out at 37 °C.

PLA. Following permeabilization, cells were blocked in blocking solution (Sigma) for 1 h at 37 °C and then incubated in blocking solution with primary antibodies for 1 h at 37 °C. After being washed with wash buffer A (Sigma), cells were incubated with PLUS and MINUS PLA probes (Sigma) for 1 h at 37 °C and washed with wash buffer A (Sigma). Ligation was performed by incubating the cells with ligase diluted in ligation buffer (Sigma) for 30 min at 37 °C. After washing with wash buffer A (Sigma), amplification was carried out at 37 °C for 1 h with polymerase diluted in amplification solution (Sigma) and protected from light. Cells were then washed two times in wash buffer B, one time in 0.01× wash buffer B, then incubated and mounted with Duolink mounting media with DAPI (Sigma). Tubulin was labeled with a fluorescent derivative of paclitaxel, Oregon Green 488 paclitaxel (Thermo Fisher Scientific).

Data Availability. All study data are included in the article and supporting information.

ACKNOWLEDGMENTS. This work was supported by grants from Associazione Italiana per la Ricerca sul Cancro (IG13074) and Telethon (GGP11176), l'Institut National du Cancer (INCA-PLBIO17-043), the Project International de Coopération Scientifique–CNRS (n°6824) and l'Association pour la Recherche contre le Cancer (130607082). Confocal analysis was performed at the Centro Grandi Apparecchiature of the University of Tuscia. We also thank A. Epanchitsev for providing the CS cell lines. We thank Izabela Sumara, Manuel Mendoza, Evanthia Pangou, Emanuel Compe, and Frederic Coin for fruitful discussions.

1. P. C. Hanawalt, G. Spivak, Transcription-coupled DNA repair: Two decades of progress and surprises. *Nat. Rev. Mol. Cell Biol.* **9**, 958–970 (2008).
2. D. B. Bregman *et al*., UV-induced ubiquitination of RNA polymerase II: A novel modification deficient in Cockayne syndrome cells. *Proc. Natl. Acad. Sci. U.S.A.* **93**, 11586–11590 (1996).
3. J. Q. Svejstrup, Rescue of arrested RNA polymerase II complexes. *J. Cell Sci.* **116**, 447–451 (2003).
4. J. P. Lainé, J. M. Egly, When transcription and repair meet: A complex system. *Trends Genet.* **22**, 430–436 (2006).
5. Y. van der Weegen *et al*., The cooperative action of CSB, CSA, and UVSSA target TFIIH to DNA damage-stalled RNA polymerase II. *Nat. Commun.* **11**, 2104 (2020).
6. K. A. Henning *et al*., The Cockayne syndrome group A gene encodes a WD repeat protein that interacts with CSB protein and a subunit of RNA polymerase II TFIIH. *Cell* **82**, 555–564 (1995).
7. C. Troelstra *et al*., ERCC6, a member of a subfamily of putative helicases, is involved in Cockayne's syndrome and preferential repair of active genes. *Cell* **71**, 939–953 (1992).
8. A. C. Karikkineth, M. Scheibye-Knudsen, E. Fivenson, D. L. Croteau, V. A. Bohr, Cockayne syndrome: Clinical features, model systems and pathways. *Ageing Res. Rev.* **33**, 3–17 (2017).
9. L. Proietti-De-Santis, P. Drané, J. M. Egly, Cockayne syndrome B protein regulates the transcriptional program after UV irradiation. *EMBO J.* **25**, 1915–1923 (2006).
10. C. P. Selby, A. Sancar, Cockayne syndrome group B protein enhances elongation by RNA polymerase II. *Proc. Natl. Acad. Sci. U.S.A.* **94**, 11205–11209 (1997).
11. J. Bradsher *et al*., CSB is a component of RNA pol I transcription. *Mol. Cell* **10**, 819–829 (2002).
12. X. Yuan, W. Feng, A. Imhof, I. Grummt, Y. Zhou, Activation of RNA polymerase I transcription by cockayne syndrome group B protein and histone methyltransferase G9a. *Mol. Cell* **27**, 585–595 (2007).
13. S. Feuerhahn, J. M. Egly, Tools to study DNA repair: What's in the box? *Trends Genet.* **24**, 467–474 (2008).
14. E. Citterio *et al*., ATP-dependent chromatin remodeling by the Cockayne syndrome B DNA repair-transcription-coupling factor. *Mol. Cell. Biol.* **20**, 7643–7653 (2000).
15. N. L. Batenburg *et al*., ATM and CDK2 control chromatin remodeler CSB to inhibit RIF1 in DSB repair pathway choice. *Nat. Commun.* **8**, 1921 (2017).
16. C. Zhang, F. Zhang, The multifunctions of WD40 proteins in genome integrity and cell cycle progression. *J Genomics* **3**, 40–50 (2015).
17. R. Groisman *et al*., The ubiquitin ligase activity in the DDB2 and CSA complexes is differentially regulated by the COP9 signalosome in response to DNA damage. *Cell* **113**, 357–367 (2003).
18. E. S. Fischer *et al*., The molecular basis of CRL4DDB2/CSA ubiquitin ligase architecture, targeting, and activation. *Cell* **147**, 1024–1039 (2011).
19. A. Epanchintsev *et al*., Cockayne's syndrome A and B proteins regulate transcription arrest after genotoxic stress by promoting ATF3 degradation. *Mol. Cell* **68**, 1054–1066.e6 (2017).
20. Y. Nakazawa *et al*., Ubiquitination of DNA damage-stalled RNAPII promotes transcription-coupled repair. *Cell* **180**, 1228–1244.e24 (2020).
21. A. Tufegdžić Vidaković *et al*., Regulation of the RNAPII pool is integral to the DNA damage response. *Cell* **180**, 1245–1261.e21 (2020).
22. K. Son, O. D. Schärer, Repair, removal, and shutdown: It all hinges on RNA polymerase II ubiquitylation. *Cell* **180**, 1039–1041 (2020).

23. R. A. Green, E. Paluch, K. Oegema, Cytokinesis in animal cells. *Annu. Rev. Cell Dev. Biol.* **28**, 29–58 (2012).
24. B. Mierzwa, D. W. Gerlich, Cytokinetic abscission: Molecular mechanisms and temporal control. *Dev. Cell* **31**, 525–538 (2014).
25. M. Agromayor, J. Martin-Serrano, Knowing when to cut and run: Mechanisms that control cytokinetic abscission. *Trends Cell Biol.* **23**, 433–441 (2013).
26. V. Nähse, L. Christ, H. Stenmark, C. Campsteijn, The abscission checkpoint: Making it to the final Cut. *Trends Cell Biol.* **27**, 1–11 (2017).
27. F. A. Barr, U. Gruneberg, Cytokinesis: Placing and making the final cut. *Cell* **131**, 847–860 (2007).
28. P. Steigemann, D. W. Gerlich, Cytokinetic abscission: Cellular dynamics at the midbody. *Trends Cell Biol.* **19**, 606–616 (2009).
29. V. Laugel *et al*., Mutation update for the CSB/ERCC6 and CSA/ERCC8 genes involved in Cockayne syndrome. *Hum. Mutat.* **31**, 113–126 (2010).
30. J. E. Cleaver, V. Bezrookove, I. Revet, E. J. Huang, Conceptual developments in the causes of Cockayne syndrome. *Mech. Ageing Dev.* **134**, 284–290 (2013).
31. L. V. Mayne, A. Priestley, M. R. James, J. F. Burke, Efficient immortalization and morphological transformation of human fibroblasts by transfection with SV40 DNA linked to a dominant marker. *Exp. Cell Res.* **162**, 530–538 (1986).
32. M. Murata-Hori, M. Tatsuka, Y. L. Wang, Probing the dynamics and functions of aurora B kinase in living cells during mitosis and cytokinesis. *Mol. Biol. Cell* **13**, 1099–1108 (2002).
33. R. Groisman *et al*., CSA-dependent degradation of CSB by the ubiquitin-proteasome pathway establishes a link between complementation factors of the Cockayne syndrome. *Genes Dev.* **20**, 1429–1434 (2006).
34. P. Latini *et al*., CSA and CSB proteins interact with p53 and regulate its Mdm2-dependent ubiquitination. *Cell Cycle* **10**, 3719–3730 (2011).
35. Y. L. Juang *et al*., APC-mediated proteolysis of Ase1 and the morphogenesis of the mitotic spindle. *Science* **275**, 1311–1314 (1997).
36. C. Mollinari *et al*., PRC1 is a microtubule binding and bundling protein essential to maintain the mitotic spindle midzone. *J. Cell Biol.* **157**, 1175–1186 (2002).
37. C. Mollinari *et al*., Ablation of PRC1 by small interfering RNA demonstrates that cytokinetic abscission requires a central spindle bundle in mammalian cells, whereas completion of furrowing does not. *Mol. Biol. Cell* **16**, 1043–1055 (2005).
38. L. Capalbo *et al*., The midbody interactome reveals unexpected roles for PP1 phosphatases in cytokinesis. *Nat. Commun.* **10**, 4513 (2019).
39. N. Elia, R. Sougrat, T. A. Spurlin, J. H. Hurley, J. Lippincott-Schwartz, Dynamics of endosomal sorting complex required for transport (ESCRT) machinery during cytokinesis and its role in abscission. *Proc. Natl. Acad. Sci. U.S.A.* **108**, 4846–4851 (2011).
40. J. Guizetti *et al*., Cortical constriction during abscission involves helices of ESCRT-III--dependent filaments. *Science* **331**, 1616–1620 (2011).
41. Z. Storchova, D. Pellman, From polyploidy to aneuploidy, genome instability and cancer. *Nat. Rev. Mol. Cell Biol.* **5**, 45–54 (2004).
42. C. Lindon, J. Pines, Ordered proteolysis in anaphase inactivates Plk1 to contribute to proper mitotic exit in human cells. *J. Cell Biol.* **164**, 233–241 (2004).
43. S. Stewart, G. Fang, Destruction box-dependent degradation of aurora B is mediated by the anaphase-promoting complex/cyclosome and Cdh1. *Cancer Res.* **65**, 8730–8735 (2005).
44. E. Morita *et al*., Human ESCRT and ALIX proteins interact with proteins of the midbody and function in cytokinesis. *EMBO J.* **26**, 4215–4227 (2007).
45. E. Morita *et al*., Human ESCRT-III and VPS4 proteins are required for centrosome and spindle maintenance. *Proc. Natl. Acad. Sci. U.S.A.* **107**, 12889–12894 (2010).
46. M. Frontini, L. Proietti-De-Santis, Interaction between the Cockayne syndrome B and p53 proteins: Implications for aging. *Aging (Albany NY)* **4**, 89–97 (2012).
47. U. Kristensen *et al*., Regulatory interplay of Cockayne syndrome B ATPase and stress-response gene ATF3 following genotoxic stress. *Proc. Natl. Acad. Sci. U.S.A.* **110**, E2261–E2270 (2013).
48. M. N. Okur *et al*., Cockayne syndrome group A and B proteins function in rRNA transcription through nucleolin regulation. *Nucleic Acids Res.* **48**, 2473–2485 (2020).
49. R. J. Lake *et al*., The sequence-specific transcription factor c-Jun targets Cockayne syndrome protein B to regulate transcription and chromatin structure. *PLoS Genet.* **10**, e1004284 (2014).
50. S. Koch *et al*., Cockayne syndrome protein A is a transcription factor of RNA polymerase I and stimulates ribosomal biogenesis and growth. *Cell Cycle* **13**, 2029–2037 (2014).
51. A. Lebedev, K. Scharffetter-Kochanek, S. Iben, Truncated Cockayne syndrome B protein represses elongation by RNA polymerase I. *J. Mol. Biol.* **382**, 266–274 (2008).
52. M. C. Alupei *et al*., Loss of proteostasis is a pathomechanism in Cockayne syndrome. *Cell Rep.* **23**, 1612–1619 (2018).
53. M. Scheibye-Knudsen *et al*., Cockayne syndrome group A and B proteins converge on transcription-linked resolution of non-B DNA. *Proc. Natl. Acad. Sci. U.S.A.* **113**, 12502–12507 (2016).
54. M. D. Aamann *et al*., Cockayne syndrome group B protein promotes mitochondrial DNA stability by supporting the DNA repair association with the mitochondrial membrane. *FASEB J.* **24**, 2334–2346 (2010).
55. B. R. Berquist, D. M. Wilson 3rd, Pathways for repairing and tolerating the spectrum of oxidative DNA lesions. *Cancer Lett.* **327**, 61–72 (2012).
56. L. Chatre, D. S. Biard, A. Sarasin, M. Ricchetti, Reversal of mitochondrial defects with CSB-dependent serine protease inhibitors in patient cells of the progeroid Cockayne syndrome. *Proc. Natl. Acad. Sci. U.S.A.* **112**, E2910–E2919 (2015).
57. N. N. Fang *et al*., Rsp5/Nedd4 is the main ubiquitin ligase that targets cytosolic misfolded proteins following heat stress. *Nat. Cell Biol.* **16**, 1227–1237 (2014).
58. M. Scheibye-Knudsen *et al*., A high-fat diet and NAD(+) activate Sirt1 to rescue premature aging in cockayne syndrome. *Cell Metab.* **20**, 840–855 (2014).
59. A. Panopoulos *et al*., Failure of cell cleavage induces senescence in tetraploid primary cells. *Mol. Biol. Cell* **25**, 3105–3118 (2014).
60. D. Yang, A. Welm, J. M. Bishop, Cell division and cell survival in the absence of survivin. *Proc. Natl. Acad. Sci. U.S.A.* **101**, 15100–15105 (2004).
61. H. Tanaka *et al*., Cytokinetic failure-induced tetraploidy develops into aneuploidy, triggering skin aging in phosphovimentin-deficient mice. *J. Biol. Chem.* **290**, 12984–12998 (2015).
62. P. Vinciguerra, S. A. Godinho, K. Parmar, D. Pellman, A. D. D'Andrea, Cytokinesis failure occurs in Fanconi anemia pathway-deficient murine and human bone marrow hematopoietic cells. *J. Clin. Invest.* **120**, 3834–3842 (2010).
63. D. Dambournet *et al*., Rab35 GTPase and OCRL phosphatase remodel lipids and F-actin for successful cytokinesis. *Nat. Cell Biol.* **13**, 981–988 (2011).
64. A. J. Ridley, J. Colley, D. Wynford-Thomas, C. J. Jones, Characterisation of novel mutations in Cockayne syndrome type A and xeroderma pigmentosum group C subjects. *J. Hum. Genet.* **50**, 151–154 (2005).
65. R. Kuriyama, G. Keryer, G. G. Borisy, The mitotic spindle of Chinese hamster ovary cells isolated in taxol-containing medium. *J. Cell Sci.* **66**, 265–275 (1984).
66. Y. S. Choo, Z. Zhang, Detection of protein ubiquitination. *J. Vis. Exp.* **30**, 1293 (2009).